Semicrystalline Diblock Copolymer Platelets in Dilute Solution

Eric K. Lin† and Alice P. Gast*

Department of Chemical Engineering, Stanford University, Stanford, California 94305

Received December 19, 1995; Revised Manuscript Received March 20, 1996[⊗]

ABSTRACT: In dilute solution, semicrystalline diblock copolymers with one crystallizable block form thin platelet structures consisting of a chain-folded crystalline domain between solvated layers of the amorphous block chains. The amorphous block is attached to the crystalline fold surface, forming a model system of tethered chains at a flat interface. We use self-consistent mean field (SCF) theory and a chain-folding model to calculate both the equilibrium platelet thickness and the tethered chain density profile. The theoretical predictions are compared with small-angle X-ray (SAXS) and neutron (SANS) scattering measurements from poly(ethylene oxide)−polystyrene (PEO/PS) suspended in cyclopentane and polyethylene−poly(ethylpropylene) (PE/PEP) suspended in *n*-decane. The SCF calculations for the crystalline domain thickness are consistent with measured values for diblocks with short crystalline blocks or diblocks having strong enthalpic interactions between the two blocks. The SANS intensity from the tethered chain structure of a PE/PEP diblock is consistent with both SCF calculations and SAXS measurements.

1. Introduction

In this paper, we are interested in studying the structures formed by semicrystalline diblock copolymers having one crystallizable block in dilute solution. In contrast with amorphous diblock copolymers in a selective solvent that form spherical micellar structures, semicrystalline diblock copolymers self-assemble in solution to form large platelets consisting of a thin chain-folded lamellar domain between layers of the solvated amorphous block.[1] These diblocks illustrate the large effect local ordering has on the morphology of diblock copolymers in solution. Additionally, these structures provide a good experimental system to study tethered polymer chains. The amorphous block of the copolymer is attached to the crystalline surface by one end through the chemical junction between the two blocks. The chain-folded crystalline region leads to a dense packing of the amorphous blocks and results in highly stretched tethered chains.

Semicrystalline diblocks in dilute solution were first studied by Lotz et al.[1,2] They studied the structure of PEO/PS diblocks in an attempt to form stable crystalline domains of PEO. They observed square platelet structures with crystalline regions having the same structure as PEO homopolymers. The PS block was inferred to be expelled from the crystalline regime. The thin platelets were also more stable than pure PEO single crystals formed in the same solvents. More recent work on this diblock copolymer system was done by Cogan and Gast[3,4] studying the effect of trace amounts of water on the aggregate structure. Other groups have studied crystallizable block copolymers, but they have focused primarily on B−A−B triblock copolymers with the B block being the crystallizable block. Kawai et al. studied B−A−B triblocks consisting of PEO and poly(α-methylstyrene) and observed the formation of thin platelet structures although the domains were not as sharply defined as in the diblock case.[5] Dröscher and Smith used transient electric birefringence to study the kinetics of formation of square platelets of B−A−B triblocks consisting of PEO and poly(propylene oxide).[6] They found that the platelet thickness is monodisperse after the final structure is formed. These studies demonstrate common characteristics of semicrystalline block copolymers in solution, including the formation of a thin lamellar chain-folded crystalline domain and a stable structure.

Most of the recent experimental work on semicrystalline diblock copolymers has focused on bulk systems with the addition of moderate amounts of a solvent selective for one of the blocks. These polymeric systems form primarily well-ordered lamellar domains similar to those of amorphous diblock copolymers.[7] More recently, experiments on model polyolefin diblock copolymers have focused on the determination of scaling laws in relation to theoretical predictions.[8−10]

Few experimental data have been published on the dilute solution structure of these diblock systems even though they form an excellent model system for the study of tethered chains at a flat interface. Tethered chains at flat interfaces have been studied using adsorbed diblock copolymers,[11] diblock copolymers at the air−liquid interface,[12] or chains chemically grafted to a solid substrate.[13] For many of these systems, the effective tethering density is not high enough for analytic theories to be applicable. Also, it is difficult to independently characterize the tethering density; it must be inferred from the structures. Semicrystalline diblock copolymer platelets have the advantage of having very high tethering densities that are determined by the structure of the crystalline domain, a measurable quantity.

The theoretical analysis for semicrystalline diblock copolymer aggregates is also limited. In the initial study by the Lotz group,[1,2] the thermodynamics of the structures was not examined since they were primarily interested in the morphology. Additionally, to extract information about the relative domain sizes of each block, they assumed the PS layers outside the crystalline domains had polymer meltlike configurations. A better interpretation of the structures of the amorphous should include the physics of tethered chain systems. This is particularly important with respect to the presence of a solvent that swells the tethered chain domains. A modern analysis of semicrystalline platelets was carried out by Vilgis and Halperin[14] using simple scaling theory for the brush structure; however, they made no comparisons with experiment and their predictions were not quantitative. Most theories about sem-

† Present address: Polymers Division, National Institute of Standards and Technology, Gaithersburg, MD 20899.

[⊗] Abstract published in *Advance ACS Abstracts,* May 1, 1996.

S0024-9297(95)01871-7 CCC: $12.00

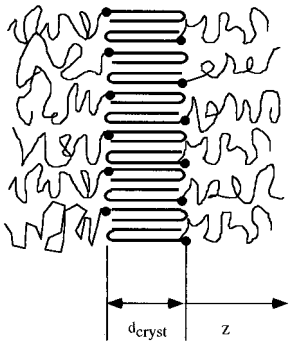

Figure 1. Schematic diagram of the model for the cross-section of semicrystalline diblock copolymer platelets.

icrystalline diblocks have concentrated on the bulk polymer systems rather than dilute solutions of platelets. In these studies, a simple chain-folding model is used to describe the crystalline domain. The differences between them come from the analysis of the amorphous block. Di Marzio et al. used a Flory description for the amorphous block entropy to calculate the equilibrium domain sizes,[15] Birshtein and Zhulina used an analytic form of the mean field equations,[16] and Whitmore and Noolandi used a self-consistent mean field (SCF) theory[17] to numerically calculate the amorphous block energy and the final equilibrium domain sizes.

In this paper, we develop a theoretical model to quantitatively calculate the equilibrium structure of both the crystalline and tethered chain domains using a self-consistent mean field approach. We also present experimental measurements of the crystalline and tethered chain regions of two semicrystalline diblock copolymer systems using small-angle scattering techniques and compare these results with the theoretical calculations.

2. Theory

2.1. Model. We model the semicrystalline aggregates as thin platelets with a flat lamellar region consisting of the chain-folded crystallizable polymer blocks between layers of the amorphous polymer blocks extending into the solvent. A schematic diagram of the cross-section of the platelet is shown in Figure 1. The separation of the two blocks in the copolymer is driven by the unfavorable interactions between them as well as by the crystallization process itself. The chemical joints between the two blocks are located in an interphase region between the crystalline and amorphous domains. As a result, the amorphous block forms a layer of chains extending into the solvent and tethered to the crystalline surface by one end.

Semicrystalline diblock copolymer aggregates differ from single crystal platelets formed by the corresponding homopolymers because the diblock aggregates appear to have an equilibrium structure whereas the homopolymer crystalline structure is kinetically controlled. This is inferred from the greater stability and more perfect structure seen in PEO/PS diblock copolymer crystallites than in pure PEO systems.[2]

A simple argument illustrates the expected equilibrium structure for the semicrystalline aggregates. We focus on the energetic contributions determining the equilibrium thickness of the crystalline domain, d_{cryst}. The primary contribution from the crystalline block is the energy needed to create a crystalline fold. Each fold has a high energetic cost and the crystalline block reduces the total free energy by creating fewer folds, resulting in a larger crystalline domain thickness. The tethered polymer chain layers can lower the total free energy by decreasing the amount of chain stretching by creating a greater number of folds and a smaller crystalline domain thickness. The energetic balance between these two effects results in an equilibrium value for d_{cryst}. The structure of the amorphous polymer layer is determined by the geometric constraints between the two domains, the amorphous block characteristics, and the solvent quality.

The dimensions of the equilibrium aggregate structure for a monodisperse semicrystalline diblock copolymer with N_A monomers of the amorphous block and N_B monomers in the crystallizable block can be calculated by minimizing the free energy with respect to d_{cryst}. Since we focus on dilute solutions with no interactions between the platelets, we ignore concentration effects on the aggregation behavior and minimize the Helmholtz free energy of an extended lamellar domain. A general form of the equation for the free energy for a semicrystalline platelet structure is given by

$$\frac{F_{tot}}{kT} = F_{cryst} + F_{amorph} + F_{interface} \tag{1}$$

where k is the Boltzmann constant and T is the temperature. The specific expressions for each term in eq 1 used in our model are similar to other theoretical treatments[14] and follow most closely the approach of Whitmore and Noolandi.[17]

2.1.1. Crystalline Block Energy. The first term F_{cryst} represents the free energy contribution from the formation of the crystalline lamellar domain. We use a phenomenological chain-folding model for F_{cryst}. We do not perform a molecular-level calculation of the energetics of a chain-folded polymer. The chain-folding model is general enough to include the fundamental characteristics of all crystalline polymers and can be adapted to describe a specific chain-folded crystalline structure. The free energy expression in units of kT per chain is

$$F_{cryst} = -\Delta H_f N_B + n_f E_{fold} \tag{2}$$

where ΔH_f is the overall heat of fusion per monomer of the crystallizable block, n_f is the number of folds within one polymer, and E_{fold} is the fold energy. In this expression, the overall heat of fusion is independent of the size of the crystalline domain, depending only on the length of the crystalline block. As a result, the heat of fusion is a constant in the minimization of F_{tot} with respect to d_{cryst} and only the fold energy, E_{fold}, is relevant.

The number of folds for the crystallizable block, n_f, determines the parameters characterizing the amorphous tethered chain block as well as d_{cryst}. The specific values are obtained geometrically from the crystalline unit cell structure with dimensions a, b, and c. By convention, the c dimension represents the unit cell size perpendicular to the fold plane and the other two dimensions represent directions parallel to the fold plane. The crystalline domain size, d_{cryst}, is given by

$$d_{cryst} = \frac{N_B c}{n_c(n_f + 1)} \tag{3}$$

where n_c is the number of monomers through the c axis of the unit cell. The nondimensional grafting density,

σ, for the tethered chain layer is

$$\sigma = \frac{1}{2}\frac{b_A{}^2 n_{chains}}{(n_f + 1)ab} \tag{4}$$

where n_{chains} is the number of polymer chains per unit cell of the crystalline polymer block, ab represents the surface area of the crystalline unit cell, and b_A is the statistical segment length of the tethered polymer chain. The factor of $^1/_2$ is present because only half of the tethered chains appear on each side of the crystalline layer.

In developing these expressions, we have implicitly assumed 100% crystallinity in the chain-folded domain and adjacent re-entry for the folded polymer chain. These assumptions are geometric ones made to relate the crystalline block structure to that of the amorphous block through σ. The values for real systems are not expected to differ greatly from these conditions. As a result, the amorphous block energy may be changed from the small variations in σ, but the crystalline fold energy is not affected as we use experimentally determined values already including the imperfections within a crystalline domain. We also assume the ends of the crystallized chain are located at the fold surfaces and not within the crystalline domain. There is an energetic penalty for the inclusion of the amorphous block or chain in the crystalline region, but in real systems, some degree of noncrystallinity is expected. Nevertheless, we expect the fold distances calculated here for the fully crystalline domain provide a good estimate for d_{cryst}. In contrast with bulk semicrystalline systems, homopolymer single crystals have higher crystallinities and more adjacent re-entry folds,[18] so our approximations here may not be unreasonable. We have also assumed the presence of only one crystalline layer, although it has been suggested that there could be two crystalline layers pressed together for the PEO/PS diblock copolymer.[2] The presence of more than one layer would affect the absolute size of the crystalline thickness and the $^1/_2$ prefactor in eq 4, but does not change the scaling of d_{cryst} with respect to the system characteristics.

2.1.2. Amorphous Block Energy. The second term in eq 1, F_{amorph}, represents the free energy of the tethered chain layers. As previously noted, the amorphous chains of the diblock copolymer are highly extended because of the relatively high grafting densities at the crystalline−amorphous block interface. Given the planar geometry and parameters set by the crystalline domain, F_{amorph} can be calculated using self-consistent mean field (SCF) theory. We can then determine the structure of the tethered chain layer as well as quantitatively calculate the free energy without ignoring scaling prefactors.[14]

The fundamental quantity to be calculated in mean field studies is the polymer segment probability distribution function, $G(z,z'|t)$, representing the probability of finding segment t at the position z, given that the segement started at the position z'. The polymer chain is modeled as a random walk in a potential field. From this description, the probability distribution function, G, is governed by the forced diffusion equation[19]

$$\frac{\partial G}{\partial t} - \frac{b_A{}^2}{6}\nabla^2 G + \omega(z)G = \delta(t)\delta(z-z') \tag{5}$$

where ω is the mean field potential. In this equation, the connectivity of the polymer chain enters through t and the potential term accounts for the average interaction of one polymer chain with all other polymer chains.

Once G is calculated, the volume fraction profile of the tethered chain layer is described by

$$\phi_A(z) = \frac{\rho_A(z)}{\rho_{A0}} = \frac{C}{\rho_{A0}W}\int_0^N \mathrm{d}t\, G(0,z|t)\int_0^\infty \mathrm{d}z'\, G(z,z'|N-t) \tag{6}$$

where

$$W = \int_0^\infty \mathrm{d}z'\, G(0,z'|N) \tag{7}$$

is the configurational partition function for a tethered polymer chain, ρ_{A0} is the bulk number density of the polymer segments, and $\rho_A(z)$ is the local number density at z. Equation 6 can be interpreted as the normalized convolution of two probability distribution functions, one describing a polymer segment of length t starting at the surface and ending at the position z and one describing a polymer segment of length $N - t$ starting in the bulk and also ending at the position z. The normalization constant C ensures conservation of polymer segments. The solution is assumed to be locally imcompressible and the volume fraction of the solvent is $\phi_s(z) = 1 - \phi_A(z)$.

The self-consistency in the equations arises from the direct relationship between the volume fraction profiles and the mean field potential, ω, through

$$\omega(z) = \frac{\rho_{s0}}{\rho_{A0}}\{-\ln \phi_s(z) + \chi[\phi_s(z) - \phi_A(z)]\} \tag{8}$$

where ρ_{s0} is the bulk number density of solvent molecules and χ is the Flory−Huggins interaction parameter.[17,20] The mean field potential can be interpreted as the local solvent excess chemical potential and represents the energy associated with replacing a solvent molecule by a polymer segment.

The free energy of the amorphous block layer is then[17]

$$F_{amorph} = -\ln W - \frac{\rho_{s0}}{\sigma}\int_0^\infty (-\ln \phi_s(z) - \chi\phi_A{}^2(z))\, \mathrm{d}z \tag{9}$$

a term from the single-chain partition function and a correction for an overcounting of the segment−segment interactions arising in mean field theories.[21]

The remaining term in eq 1, $F_{interface}$, represents the free energy from the interfacial region between the crystalline and amorphous domains. This energy arises from the interaction energy between the chemically different blocks and includes surface energies not only at the fold surface but also at the edges of the platelet. In our calculations, we assume this term and its variation with d_{cryst} are negligible with respect to F_{amorph} and F_{cryst}. If the interfacial energy was large, the aggregates would minimize this energy by decreasing the surface area of the platelet structure. In the PEO/PS system, the lateral dimensions of the platelets are on the order of a micron whereas the typical size of the crystalline domain is on the order of 100 Å. As a result, there are only small variations in the total crystalline surface area with respect to d_{cryst}. Also, the SCF calculations for the pure semicrystalline diblock copolymer by Whitmore and Noolandi[17] show that $F_{interface}$ is almost constant with respect to the crystalline domain thickness and that the dominant energetic contributions arise from F_{amorph} and F_{cryst}.

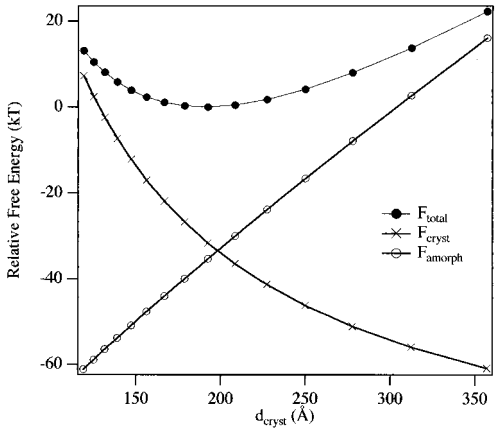

Figure 2. Relative free energies from the crystalline block and amorphous block as a function of the crystalline domain thickness. The minimum in the total free energy represents the equilibrium structure of the platelet.

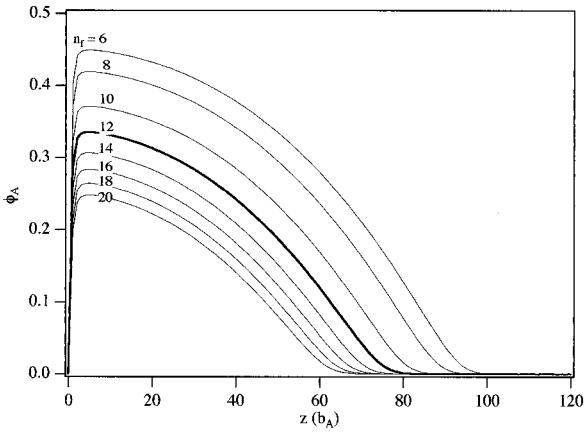

Figure 3. Volume fraction profiles of the possible tethered chain structure for different numbers of crystalline folds. The equilibrium profile is given by the bold line.

2.2. Theoretical Calculations. In this section, we calculate the equilibrium structure from the free energy equation and examine the variation of the structural dimensions with the polymer system characteristics. We also make comparisons with predictions from scaling theory.[14] The parameters we use here are not representative of a particular polymeric system but are of the same order of magnitude as the polymers we study experimentally and are chosen to illustrate results from the theoretical model.

An example of the minimum in the overall free energy as a function of the crystalline domain size is shown in Figure 2 along with contributions from F_{amorph} and F_{cryst}. The curves in Figure 2 have been shifted for clarity. These results are for a semicrystalline diblock copolymer in solution with $N_A = 200$, $N_B = 500$, $\chi = 0.0$, and $\rho_s = \rho_A = 1.0$. For the crystalline unit cell structure, we choose a statistical segment length of $b_A = 5.0$ Å, $c = 5.0$ Å, $ab = 25.0$ Å^2, and $E_{fold} = 2.0 \times 10^{-20}$ J. The total free energy, F_{tot}, has a minimum at $d_{cryst} = 192$ Å, corresponding to 12 folds per crystallizable diblock copolymer. Although the energy appears to fall upon a continuous curve, it is important to remember that d_{cryst} is calculated only for integral numbers of folds.

Once the free energy is minimized, the equilibrium structure of the tethered chain layer is determined. The volume fraction profiles, ϕ_A, as a function of distance from the interface for integral values of n_f are shown in Figure 3. The number of crystalline folds determines the tethering density, producing a family of allowable volume fraction profiles for this particular system. As the number of folds increases, the tethering density drops. The overall size of the tethered chain layer and the maximum volume fraction in the density profiles then decrease, indicating that the polymer layer becomes more diffuse with less highly stretched chains.

It is of interest to see if the theoretical results approach the limiting power law behavior predicted from scaling arguments. We compare the SCF calculations with results from the scaling theory developed by Vilgis and Halperin[14] and results from mean field scaling arguments. The Vilgis and Halperin results came from a free energy minimization similar to the one used here; however, they used the scaling "blob" ansatz to describe the tethered chain energetics. In addition to the flat lamellar structure, they analyzed finite-sized crystalline domains using the spherical and cylindrical geometries to scale the energy in the amorphous block; however, we are only interested in the lamellar results. The scaling law for lamellar structures in an athermal solvent is given by

$$d_{cryst} \approx N_B N_A^{-6/11} E_{fold}^{6/11} \tag{10}$$

It is known that the free energy scaling of tethered polymer chains using the blob ansatz is slightly different in the mean field approximation.[22,23] The resulting scaling relationship from the mean field approximation is

$$d_{cryst} \approx N_B N_A^{-3/5} E_{fold}^{3/5} \tag{11}$$

These two approximations for athermal solvents result in slightly different power law dependences of d_{cryst} on N_A and E_{fold} in contrast with the identical scaling laws for the tethered chain layer size. For each case, the crystalline domain size scales linearly with N_B because only the number of folds is important for the equilibrium structure. Given a constant amorphous block length, the number of folds remains constant and d_{cryst} increases linearly with the length of the crystalline block. The scaling law also shows that d_{cryst} decreases with increasing amorphous block length N_A because the increased stretching energy produces more folds per diblock. The thickness also decreases as the fold energy E_{fold} decreases because more crystalline folds can be accommodated to relieve the stretching energy of the tethered chains. These scaling results are easily extended to describe platelets in a Θ solvent, resulting in the relationship

$$d_{cryst} \approx N_B N_A^{-1/2} E_{fold}^{1/2} \tag{12}$$

These scaling laws are not quantitative but provide qualitative relationships between the relevant system parameters at the appropriate limits.

In Figure 4 we show the calculated equilibrium values of d_{cryst} for the same parameters used in Figure 2, while varying N_A in both an athermal solvent, $\chi = 0.0$ and a Θ solvent, $\chi = 0.5$. The equilibrium values of d_{cryst} do not fall on a smooth line because of the restriction to integral values of folds per chain. As N_A increases, an increase in number of folds or a decrease in d_{cryst} does not occur until the stretching energy increases enough to cause the crystalline block to create another fold. Experimental evidence for these quantized changes in the crystalline domain thickness was presented by

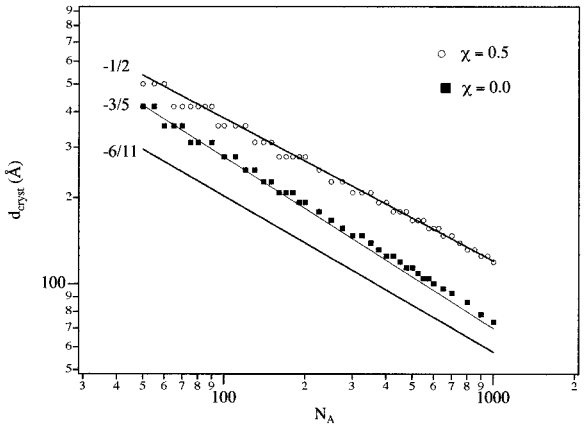

Figure 4. Equilibrium crystalline domain thickness as a function of the degree of polymerization of the tethered polymer for two solvent conditions. The results are compared with the scaling predictions[14] given by the solid lines.

Gervais and Gallot for nearly bulk PEO/PS diblock copolymer systems while varying the concentration of a selective solvent.[24] If the crystalline block has a small integral number of folds, the scaling laws will not fit well because each fold causes relatively large jumps in the thickness. The scaling relationships are only applicable for cases where the amorphous and crystalline blocks are long enough to provide a quasi-continuous distribution of crystalline thickness as a function of the number of folds. The predicted scaling values compare very well with the SCF results, indicating that the numerical calculations have the expected behavior for the limiting cases of an athermal solvent and a Θ solvent. Naturally, the self-consistent mean field calculations for the athermal solvent system more closely approach the $-3/5$ power law dependence of the mean field scaling, but the differences with the blob model are very small. Real systems are expected to lie somewhere in between the two limits in solvent quality, although the differences at these limits are very small and may be difficult to distinguish from the available scaling laws.

Experimental Section

We measure the characteristic dimensions of two types of semicrystalline diblock copolymers using small-angle X-ray (SAXS) and neutron (SANS) scattering experiments. We compare the thickness of the crystalline domain and the structure of the tethered chain layer with predictions from the SCF theory outlined above.

3.1. Polymer Characteristics. To experimentally study semicrystalline diblock copolymer platelets, we use two different diblocks, poly(ethylene oxide)−polystyrene (PEO/PS) and polyethylene−poly(ethylpropylene) (PE/PEP). The PEO and PE blocks are the crystallizable blocks and PS and PEP are the amorphous blocks. We suspend both polymers in low molecular weight solvents selective for the amorphous block and measure the characteristics of the aggregates through small-angle scattering techniques. The physical properties of the polymers used in this study are summarized in Table 1, including molecular weights, polydispersities, and weight fractions of the crystallizable block. Some of the blocks are deuterated and are indicated with a lower case d in the sample name.

The PEO/PS diblock copolymer was purchased from Polymer Laboratories, Inc. Dilute solutions of the PEO/PS diblock were made by dissolving the polymer in cyclopentane, a selective solvent for polystyrene, purchased from Eastman Kodak. To observe large platelet aggregates, it is important to remove all trace amounts of water.[3] Trace amounts of water dissolve the crystalline block, destroying the crystalline structure and producing spherical micellar structures.[3] We first dissolve the polymer in cyclopentane at a 1 wt % concentration and then heat to ≈70 °C, above the melting temperature of pure crystalline PEO. The clear solutions were then placed in a desiccator with the lid of the sample container slightly ajar and allowed to cool to room temperature. After several hours, large aggregates are observed consisting of semicrystalline platelets. The aggregates are large enough to settle out of solution.

Table 1. Physical Characteristics of the Semicrystalline Diblock Copolymers[a]

polymer	mol wt (kg/mol)	M_w/M_n	wt frac PEO or PE
PEO/PS			
3/8	11.14	1.12	0.26
PE/PEP			
6/d30	36	1.05	0.17
10/100	110	1.05	0.10
20/30	50	1.05	0.66
35/d90	125	1.05	0.28

[a] Two of the PE/PEP diblocks have deuterated PEP blocks and are indicated with a d in the sample name.

Table 2. Densities, Electron Densities, and Neutron Scattering Length Densities for Each Component

component	ρ (g/cm^3)	ρ^X (Å^{-3})	ρ^N ($\times 10^{-10}$ cm^{-2})
poly(ethylene oxide)	1.13	0.371	0.64
polystyrene	1.04	0.343	1.42
cyclopentane	0.742	0.255	
polyethylene	0.986	0.339	−0.360
poly(ethylpropylene)	0.854	0.294	
d-poly(ethylpropylene)	0.854	0.264	5.216
n-decane	0.73	0.254	−0.489

The PE/PEP diblock copolymers were synthesized by Dr. Lewis Fetters at the Exxon Research and Engineering Co. These diblocks were prepared via anionic polymerization of the parent polydienes[25] and then hydrogenated to form the PE/PEP diblock copolymer.[26] Some of the PEP blocks were deuterated to provide contrast in small-angle neutron scattering (SANS) experiments. The hydrogenation process leads to the formation of ≈10% ethyl branches in the PE block and ≈10% isopropyl side groups in the PEP block[27] because of the presence of both 1,2 and 1,4 double bonds in the polydienes. The PE/PEP polymers were suspended in *n*-decane at concentrations between 0.5 and 12 wt %. The polymers were dissolved in *n*-decane and then heated to 80 °C. The clear solutions were slowly cooled to room temperature. After several hours, the solutions became slightly turbid, indicating that crystalline aggregates had formed. The particles were not large enough to settle out of solution.

3.2. Small-Angle Scattering. We study semicrystalline platelet structures, using small-angle X-ray (SAXS) and neutron (SANS) scattering to measure d_{cryst} and ϕ_A. The scattered radiation from a sample at an angle θ from the beam path probes the structure on the length scale of q^{-1}, where $q = (4\pi/\lambda)\sin(\theta/2)$ and λ is the wavelength of the probing radiation. Different wavelengths and/or radiation sources are used to provide variations in contrast and in the accessible q range. The strength of the scattering depends upon the difference between the scattering length densities of the particles and the solvent. The densities, electron densities, and the neutron scattering lengths of the components in this study are shown in Table 2.

3.2.1. X-ray. The small-angle X-ray scattering (SAXS) experiments were performed at the Stanford Synchrotron Radiation Laboratory (SSRL) on beamline 1−4. Details about the station are available elsewhere.[28] The wavelength of the incident radiation was $\lambda = 1.493$ Å, and the scattered intensities were measured using a Reticon 1024 pixel linear photodiode array cooled to −80 °C. The X-ray beam was collimated using two sets of slits to reduce parasitic scattering. The sample to detector distance was set between 52 and 107 cm for a q range between 0.005 and 0.18 Å^{-1}. The magnitudes of scattering vector were calibrated using chicken tendon collagen (domain spacing, $d = 653$ Å). Typically, eight or nine peaks

were observed and the q range was calibrated using the prominent sixth peak.

The polymer solutions were loaded into 1 mm thick sample cells with Kapton windows. The measured intensities were first normalized by the sample transmission, thickness, and the incident intensity. The signal from the suspended particles was obtained by subtracting the solvent scattering from the sample scattering. The data were then placed on an absolute scale with reference to a Lupolen standard.[29] All experiments were performed at room temperature.

3.2.2. Neutron. The small-angle neutron scattering (SANS) experiments were performed at the National Institute of Standards and Technology (NIST) on beamline NG7. The details of the experimental setup are described elsewhere.[30] The incident radiation had a wavelength of 7 Å ($\Delta\lambda/\lambda = 0.11$ at full width, half-maximum). The sample to detector distance was 13.31 m for a range of q between 0.004 and 0.038 Å^{-1}. The polymer solutions were loaded into 1 mm thick quartz cells. Again, the intensity data of interest were obtained by subtracting the solvent scattering from that of the sample. The data were put on an absolute scale with the NIST silica standard using standard reduction techniques. All experiments were performed at room temperature.

4. Results and Discussion

4.1. Model Parameters. We calculate the equilibrium structure of the semicrystalline aggregates for these diblock copolymer systems and compare the results with those from the scattering experiments. There are a number of parameters that are needed for the calculation including the crystalline polymer unit cell structure, the physical characteristics of the amorphous polymer block, and the Flory−Huggins χ parameter.

4.1.1. Crystalline Blocks. For both diblock copolymer systems, the chain-folded structure in the crystalline domain is the same as that of the analogous homopolymer. Rangarajan et al. performed wide-angle X-ray scattering (WAXS) on bulk PE/PEP systems and found that the crystalline structure in the lamellar domains is the same as that of bulk PE homopolymers.[8] Lotz et al. used electron diffraction techniques and determined that the crystalline structure of the PEO/PS system is the same as that of pure PEO.[2]

Crystalline PE has an orthorhombic unit cell structure with $c = 2.5$ Å, $a = 7.5$ Å, and $b = 4.9$ Å. Each unit cell contains two polymer chains and two carbon units through the c axis perpendicular to the plane of the platelet.[18] These values are slightly larger than those found in pure polyethylene and are taken from a study by Howard et al. measuring the unit cell dimensions for polyethylene with some ethyl branches[31] arising from the polymerization of the polydiene. The unit cell structure of PEO is monoclinic[32] with the c axis being 19.3 Å in length. The a and b dimensions are 8.15 and 12.99 Å, respectively. Within each PEO unit cell, there are four polymer chains in a helical configuration with seven monomers going through two turns.

The crystalline fold energies were taken from experimental data from the melting point depression of both single crystal and bulk crystalline samples. By measuring the melting point depression of homopolymer platelets relative to that of an infinite crystal and using an equilibrium free energy expression for the formation of a single chain-folded crystal, one can determine the fold energy from the slope of the degree of melting point depression as a function of the thickness of the initial homopolymer crystal. The measured values for E_{fold} for polyethylene are almost identical for solution-growth crystals, dried single crystals, and melt-crystallized polymers.[33] The experimental consistency provides confidence in the application of the literature values of E_{fold} to the semicrystalline diblock copolymer system. The crystalline fold energy for PEO is $E_{fold} = 1.6 \times 10^{-20}$ J and that for PE is $E_{fold} = 3.08 \times 10^{-20}$ J.[33] It is important to recall that these fold energies include the presence of nonadjacent re-entry folds in the crystalline domain. The assumptions of 100% crystallinity and adjacent re-entry affect only the value of σ used to calculate the amorphous free energy.

4.1.2. Amorphous Blocks. The parameters needed in the SCF calculations for the tethered amorphous blocks are determined by the structure of the crystalline domain. Our calculations are performed nondimensionally so we scale all lengths for the SCF calculations on the statistical segment length, b_A, of the amorphous polymer block. The statistical segment length is determined from the expression for the radius of gyration, R_g, for a Gaussian polymer coil

$$R_g = b_A\left(\frac{N_A}{6}\right)^{1/2} \tag{13}$$

R_g can be measured through scattering techniques, and given the molecular weight of the polymer, N_A and b_A are adjusted to match experimental data. For the PEP polymer block, we follow Bates et al.[27] and take b_A to be 7.2 Å. We then use experimental data measuring R_g for deuterated PEP in a hydrogenated PEP matrix[34] and determine the Kuhn ratio, the number of monomers per statistical segment, to be 0.81 monomers per b_A, thus producing the number of statistical segments for each polymer system. For the polystyrene block in cyclopentane, we use $b_A = 15.5$ Å as determined by Vagberg et al.,[35] which is consistent with light scattering data.[36] The Kuhn ratio for PS is 5.0 monomers per b_A. The densities for the monomers and the solvent are also scaled on b_A^3 for consistency. The last parameter needed for the SCF calculations is the Flory−Huggins χ parameter. For PS in cyclopentane, $\chi = 0.45$[37] and for PEP in n-decane, $\chi = 0.3$.[37]

4.2. Crystalline Domain Thickness. To compare with the theoretical calculations, we measure the size of the crystalline domain using the scattered intensity from dilute solutions of the diblock copolymers. Planar particles in solution have a scattered intensity that should be multiplied by q^2 to account for the form of flat particles with a thin cross-section. This factor arises because the particle contributes to the scattered intensity only when q is perpendicular to the plane of the particle.[38] The traditional Guinier approximation used to determine the overall particle size from small values of q has a two-dimensional analog. The Guinier approximation for thin homogeneous flat particles is

$$I_{flat}(q) = A\frac{2\pi}{q^2}(\Delta\rho^X)\tau^2 e^{(-q^2R_\tau^2)} \tag{14}$$

where A is the planar area of the particle, $\Delta\rho^X$ is the relative electron density of the platelet to the solvent, τ is the thickness of the flat particle, and R_τ is the one-dimensional radius of gyration taken from the center of the platelet perpendicular to the face as

$$R_\tau^2 = \frac{\int \Delta\rho^X(z) z^2 \, dz}{\int \Delta\rho^X(z) \, dz} \tag{15}$$

where z is the distance from the center plane of the

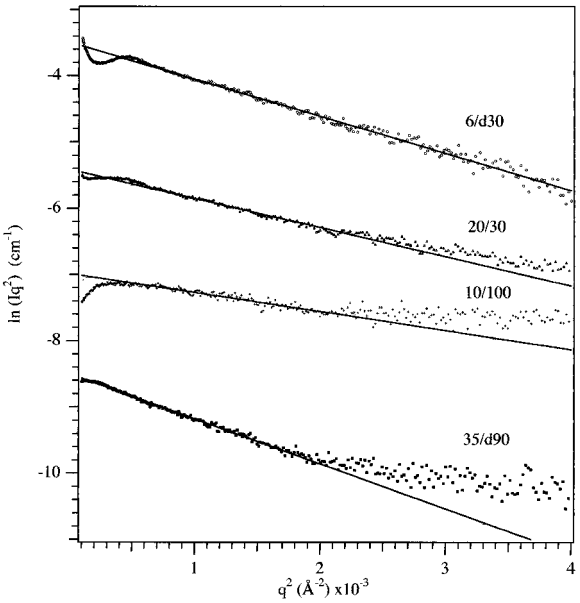

Figure 5. SAXS data from semicrystalline platelets in a Guinier thickness plot to determine the crystalline domain thicknesses. The data for each polymer are offset for clarity.

platelet. From eq 14, the slope of the linear region in a plot of $\ln(Iq^2)$ vs q^2 gives R_τ. The presence of a linear region over a range of q in this type of plot is a strong characteristic feature of flat platelets. The Guinier thickness approximation is valid for $2\pi/A < q < 1/\tau$. Deviations from the linear region for $q < 2\pi/A$ will arise as q begins to probe length scales near the size of the lateral dimensions of the particle. At higher values of q, the scattering resolves features within the platelet structure. If we assume the particle has a homogeneous electron density through the lamellar structure, the overall thickness of the particle, τ, can be calculated from R_τ through $\tau = 12^{1/2}R_\tau$.

Figure 5 shows the scattered intensity from 1 wt % solutions of the PE/PEP diblock copolymer aggregates on a Guinier thickness plot. The lamellar structure of each system is evident from the range of q where the scattered intensity is linear. The scattering profiles are similar to data used to determine the thickness of single-crystal polyethylene platelets in solution.[39] The decrease in the scattered intensity of the 10/100 and 35/d90 polymers at the lower q values is due to the finite size of the platelet structure. For the 6/d30 and 20/30 diblocks, a slight peak in the curves is present at low values of q. Although the peak is not seen in the previous two samples, this deviation most likely results from the finite size of the platelet particles and occurs where $1/q \sim$ the lateral size. The presence of a local maximum in the scattering profile suggests that the 6/d30 and 20/30 aggregates are not as large laterally as the 10/100 and 35/d90 polymers. At low enough values of q, scattering peaks characteristic of the finite size of the 35/d90 and 10/100 aggregates should also be seen. Although the Guinier thickness approximation is developed for infinitely wide lamellar particles, Pilz[40] has shown that the particle thickness determined from a Guinier plot is adequate for particles with lateral dimensions only 2 or 3 times the size of the thickness. The radius of gyration for an entire aggregate can be determined through the traditional Guinier approximation from the data when $q \rightarrow 0$. Unfortunately, we do not have data at low enough values of q to obtain information about the overall dimensions of the platelets; however, we estimate the lateral dimensions are greater than 5 times the thickness of the platelets.

Table 3. Comparison between the SCF Values for d_{cryst} and the SAXS Values Guinier Thickness Plots

polymer	N_A	N_B	d_{cryst} (Å) SAXS	d_{cryst} (Å) SCF	n_f SCF	σ SCF
PEO/PS						
3/8	16	65	62 ± 10	55	3	3.74[a]
PE/PEP						
6/d30	475	215	78 ± 6	68	7	0.17
20/30	530	714	73 ± 7	227	7	0.17
10/100	1766	357	58 ± 7	57	15	0.09
35/d90	1426	1250	91 ± 8	227	13	0.10

[a] This value for σ appears unphysical, but results from the large size of b_A for PS relative to the fold dimensions of the PEO block.

Given the thickness radius of gyration for the diblock copolymer aggregates, further interpretation of the data depends upon the electron densities of the crystalline and tethered chain domains. For the PE/PEP system, the electron density for the crystalline PE domain is much higher than the PEP domains. From Table 2, the PE monomer has a higher scattering length density than the PEP monomer relative to *n*-decane and the crystalline domain has a denser structure than the diffuse solvated PEP block. As a result, the crystalline PE block dominates the scattered intensity at the angles in the linear region of the Guinier thickness plot. We assume a homogeneous density for the platelet structure and interpret the value of τ calculated from R_τ as an effective crystalline domain thickness, d_{cryst}. This is only an effective d_{cryst} since an interphase region exists between the two domains and the PE structure is not 100% crystalline and some contrast is present between the amorphous block and the solvent. This assumption can be tested by comparing d_{cryst} from SAXS with data from SANS experiments where the solvent scattering density is matched to that of the PEP monomer. Drs. S. L. Chang and J. S. Huang at the Exxon Research and Engineering Co. have performed the SANS experiment and measured the thickness of the aggregate structure of the 35/d90 diblock copolymer and find that $d_{cryst} = 94 \pm 12$ Å from fitting their SANS data to the form factor for polydisperse platelets.[41] The value from our SAXS measurement using a separately prepared solution is $d_{cryst} = 91 \pm 8$ Å. The excellent agreement between the two scattering experiments provides confidence in the assumptions used to calculate d_{cryst} from the SAXS data.

In Table 3, we compare the crystalline domain thicknesses calculated from the SCF theory with those measured using SAXS. Also included in Table 3 are the predicted effective grafting density of the tethered chains, σ, and number of folds, n_f, per chain. The measured values of d_{cryst} are between 50 and 100 Å, on the same order of magnitude as the thicknesses of many polymer single crystals.[18] The theoretical values of d_{cryst} and the experimental data agree for the PEO/PS, the PE/PEP 6/d30, and the PE/PEP 10/100 diblock copolymers but do not agree with the measured thicknesses of the PE/PEP 35/d90 and 20/30 diblocks. For these two polymers, the calculated d_{cryst} are larger than the measured ones by approximately a factor of 3. The theoretical model predicts that the 20/30 and 6/d30 polymers should have the same number of folds in the crystalline block because the amorphous blocks are the same size; however, we observe that the 20/30 polymer has more folds than the 6/d30 polymer. The calculations agree with the experimental data for the diblocks with

both a smaller molecular weight in the crystalline block and a smaller crystalline fraction per chain.

We attribute the discrepancy between theory and experiment for the 20/30 and 35/d90 polymers to kinetic effects during the crystallization process and effects from the presence of ethyl branches in the PE block. The comparison between experiment and theory suggests that an equilibrium platelet structure is more likely to be reached for semicrystalline diblock copolymers having strong unfavorable enthalpic interactions between the two blocks of the copolymer (PEO/PS) and diblocks with larger amorphous blocks relative to the crystalline block. Rangarajan et al. have observed that the crystallinity of bulk PE/PEP polymers is much less than 100% for diblocks with large crystalline domains due to the formation of small crystallites within the bulk crystalline region.[8] For similar reasons, the PE/PEP copolymers having larger crystallizable blocks may form crystalline domains whose thicknesses are controlled by the kinetics rather than equilibrium. The crystallization kinetics are also important for the PE/PEP systems because the two polymers do not have a strong enthalpic driving force to separate from each other. The chemical similarity between PE and PEP makes it more likely to find parts of the PEP block within the PE domains than to find PS segments within the PEO domains. If some of the structures are trapped in a kinetically determined state, annealing the diblock copolymers at temperatures closer to the crystalline melting point could induce the thickening of the crystalline domain to the equilibrium values. This behavior is analogous to single crystals of bulk polyethylene, which increase in thickness as crystallization temperatures increase.[18]

Given the simplicity of the model and the complexity of the crystallization process, the comparisons for d_{cryst} between theory and experiment are reasonable. A more detailed theory would take into account the finite size of the extended lamellae. Even with discrepancies between experiment and theory for the crystalline domain thickness, the overall structure of the platelet can be studied. Since there are geometric constraints between the crystalline domain and the tethered chain layers, we can study the amorphous layers and determine whether the tethered chain structure is consistent with the measured values of d_{cryst} as well as with the tethered chain structure predicted by the mean field calculations.

4.3. Tethered Chain Layer. To study the tethered chain layer, we perform SANS experiments on the PE/PEP 6/d30 polymer with a deuterated PEP block. When the polymer is suspended in *n*-decane, the scattering length density of the solvent closely matches that of the PE block and the scattered intensity comes from the structure of the deuterated PEP block. Given the platelet structure, the structure of the tethered chain layer can be analyzed using equations developed by Auvray and Auroy for the scattering from planar interfaces.[13]

The total scattered intensity for the diblock copolymer system can be separated into three contributions corresponding to the interference between different components as

$$I(q) = I_{BB}(q) + I_{AA}(q) + I_{AB}(q) \qquad (16)$$

where B represents the crystalline block and A represents the amorphous block.

Since we have prepared solutions with effectively zero contrast between the crystalline domain and the solvent,

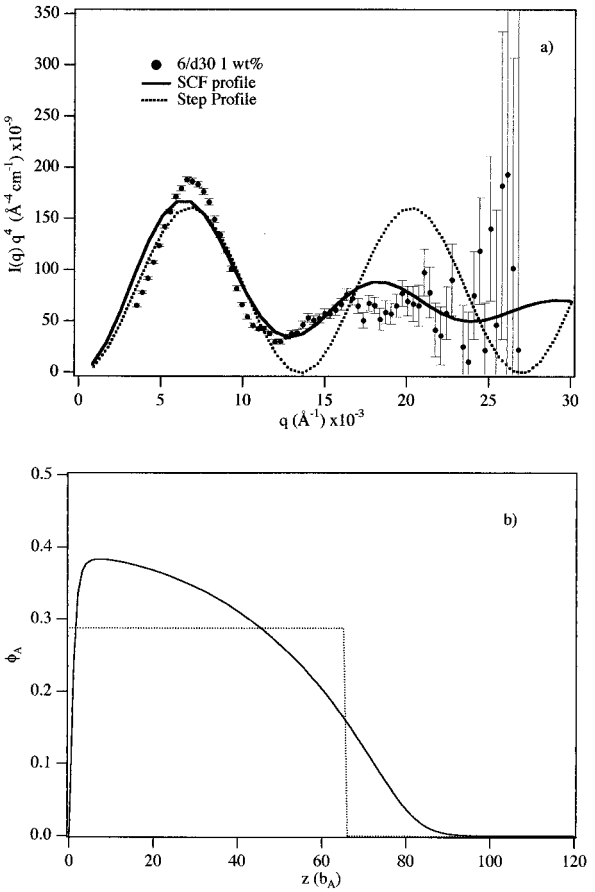

Figure 6. (a) Porod plot of the SANS data from a 1 wt % solution of PE/PEP 6/d30 platelets with the best fit SCF profile and step profile. (b) The volume fraction profiles corresponding to the fits to the experimental data.

only the I_{AA} component is of interest. The general equation for I_{AA} is given by

$$I_{AA} = 2\pi(\rho_A^N - \rho_s^N)^2 \frac{S}{V} q^{-2} \left| \int_0^\infty dz\, \phi_A(z) e^{iqz} \right|^2 + \tilde{I}_{AA}(q) \quad (17)$$

where z is the distance from the interface, S/V is the interfacial area per unit volume, and ρ_A^N and ρ_s^N are the neutron scattering length densities of the amorphous block and solvent, respectively. The first term arises from the average concentration profile of the amorphous block perpendicular to the interface, and the second term $\tilde{I}_{AA}$ arises from concentration fluctuations within the tethered chain layer. At large values of q, the Porod limit is reached where the scattering from the interface between the solid and the solvent dominates. At this limit, the scattered intensity is described by

$$I(q) = 2\pi(\rho_A^N - \rho_s^N)^2 \frac{S}{V} \frac{1}{q^4} \qquad (18)$$

Using this general formalism, Auvray et al. have calculated analytic expressions for the parabolic and step profiles.[13,42] They find that the parabolic profile with some minor modifications well describes SANS data from polystyrene chains chemically grafted to porous silica.[42]

In Figure 6 we present the scattered intensity from the tethered chain structure of the 1 wt % PE/PEP 6/d30 sample. The larger deuterated diblock, 35/d90, could not be studied because the appropriate q range was not accessible. The SANS data are best presented in a

Porod presentation of Iq^4 vs q because it emphasizes the local singularities in the concentration profile and the deviations from the Porod limit given in eq 18. The observed oscillations in the scattering profile are characteristic of an interfacial layer and are similar to the data obtained by the French group for polymer chains grafted in porous silica.[43] We have also divided the scattered intensity of the 0.5, 2, and 3 wt % solutions by the polymer concentration and see identical scattering curves, indicating that we observe single-particle scattering at these concentrations. We begin to see deviations in the scattering profile with the 5 and 9 wt % samples where a weak lamellar order begins to appear.

We compare the measured intensity with the scattering curves calculated from eq 17 using the volume fraction profiles from SCF calculations and the expression for a step profile. To fit the SCF calculations to the SANS data, we fix the model parameters used to calculate the equilibrium values of d_{cryst} and vary only the effective tethering density, σ, and a constant prefactor representing the prefactors in eq 17. We also neglect the second term in eq 17, $\tilde{I}_{AA}$, because we did not have data at high enough q values to determine the background scattering of the in-plane fluctuations. The resulting volume fraction profiles from the fits are also presented in Figure 6.

The model calculations adequately fit the experimental data, and we find the effective tethering density of the PEP block to the crystalline domain to be $\sigma = 0.14$. The profile from the SCF calculations matches the data much better than the step profile. The results of the theoretical fits demonstrate the greater accuracy of the tethered chain structure from the mean field theory over the step profile. The parabolic profile was also fit to the data and closely matches the SCF curve at lower values of q but begins to deviate from the SCF curve and the SANS data at the higher q values. Deviations between the SCF curve and the SANS data are apparent at both low and high values of q. These deviations can be attributed to features of the actual tethered chain structure that are not taken into account in the model calculations. First, the model calculations have assumed a sharp tethering interface whereas in the experimental system, an interphase region between the crystalline and amorphous domains is expected. Auvray and Auroy have found that the addition of an adsorption layer at the tethering interface greatly improved model fits to the scattered intensity, particularly at higher values of q.[42] We have also neglected the in-plane fluctuations, $\tilde{I}_{AA}$, which contribute to a background that shifts some of the scattered data in the Porod plot. These fluctuation effects are more pronounced at high q values but may contribute at lower q.[13] The $\tilde{I}_{AA}$ term can be determined through contrast variation using a series of different solvent mixtures, but was not done here due to material limitations. Finally, the interfaces are not infinite as the particles have a finite surface area. At low enough values of q, the overall shape of the platelet structure can affect the scattered intensity. The finite surface area also allows long tethered chains to extend in directions not perpendicular to the plane of the particle, changing the volume fraction profiles of the polymer chains near the platelet edges.

We compare the value of σ from the fit to the SANS data with the values determined from the equilibrium SCF calculations and the measurements of d_{cryst} from the SAXS Guinier thickness plot in Table 4. These different measurements are consistent with one another with differences of only a few folds per chain. The smaller value of σ from the SCF fit to the SANS data relative to σ from the SAXS measurement is reasonable given the assumption of a 100% crystalline domain used to determine the SAXS value of d_{cryst}. In homopolymer single crystals, crystallinities of greater than 70% are rarely observed.[18] With less crystalline order, the tethering points of the experimental system are generally spaced farther apart because of defects in the structure. We would expect a smaller value of σ from fitting the data from the tethered chain than from the value extracted from the effective thickness determined from the SAXS data. Additionally, the theoretical prediction from the full SCF theory predicts a value of σ in between the two experimental ones. Given the assumptions of the theoretical model, the structure of the tethered chain layer is reasonably well described by the mean field theory.

Table 4. Comparison for σ Determined from the SCF Fit to the SANS Data, the Equilibrium SCF Calculations, and the SAXS Measurements

feature	SANS(fit)	SCF(equil)	SAXS
σ	0.14	0.17	0.20
n_f	9	7	6

5. Summary

Semicrystalline diblock copolymers in solution form platelets consisting of a chain-folded lamellar region formed by the crystalline block between solvated layers of the amorphous block. The platelets have an equilibrium structure determined by an energy balance between the cost of forming a crystalline fold favoring a thicker crystalline domain and the stretching energy of the chains extending into solution favoring a thinner crystalline domain. We experimentally and theoretically studied the platelet structures through small-angle X-ray (SAXS) and neutron scattering (SANS) and numerical self-consistent mean field (SCF) calculations.

To calculate the equilibrium structure of the platelet structure, we minimized the free energy of an extended lamellar sheet with respect to the crystalline domain thickness. We modeled the crystalline domain with a phenomenological chain-folding model. The solvated blocks were modeled as polymer chains tethered to the crystalline domain surface due to the chemical bond between the two blocks. The structures of the amorphous block and the crystalline block are geometrically dependent on one another through the chemical bond between them. We neglected the presence of an interphase region between the two domains as well as any finite size or edge effects of the platelet. These approximations are not unreasonable in light of previous experimental evidence. We calculated the equilibrium crystalline domain size as a function of the amorphous block length for an athermal and a Θ solvent and found good agreement with the scaling predictions at these limits.

We studied two semicrystalline diblock copolymer systems, poly(ethylene oxide)−polystyrene (PEO/PS) in cyclopentane and polyethylene−poly(ethylpropylene) (PE/PEP) in *n*-decane, using small-angle scattering. We found that the SCF theory is consistent with the SAXS measurements for diblock copolymers with smaller crystalline block fractions and a stronger unfavorable enthalpic interaction between the two blocks. Diblocks with larger crystalline block fractions did not follow the

predicted scaling laws for the crystalline domain size and may have kinetically controlled structural dimensions. SANS measurements on PE/PEP diblocks with deuterated PEP blocks were used to measure the structure of the tethered chain layers. We found that the SCF volume fraction profiles are consistent with both the profile expected from the SAXS measurements and a best fit volume fraction profile. The SCF calculations also fit the data much better than the step profile assumed in scaling predictions.

We have demonstrated the importance of the tethered chain structure on the equilibrium characteristics of semicrystalline diblock copolymer platelets. In the future, careful measurements of the kinetics of the platelet formation will be useful in establishing the process of reaching an equilibrium structure as well as identifying possible differences with homopolymer solution crystallization. It would also be useful to extend the theory to better incorporate a description of the crystalline−amorphous interphase region as well as finite size effects from the edges of the platelet structures. Other novel tethered chain structures may be obtained from semicrystalline diblock copolymer mixtures, leading to the formation of mixed tethered chain layers. Although the kinetics may be complicated, the tethered chain structure will still be present and have a strong effect on the final morphology.

Acknowledgment. We acknowledge the support of the National Institute of Standards and Technology, U.S. Department of Commerce, and the Stanford Synchrotron Radiation Laboratory under the U.S. Department of Energy in providing facilities used in this study. The authors gratefully thank Exxon Research and Engineering for the generous donation of several polymer samples used in this study and J. S. Huang and S. L. Chang for many helpful discussions. E.K.L. thanks the National Science Foundation for fellowship support. This work was supported in part by the MRSEC Program of the National Science Foundation under Award No. DMR-9400354.

References and Notes

(1) Lotz, B.; Kovacs, A. J. *Kolloid-Z. Z. Polym.* **1966**, *209*, 97.
(2) Lotz, B.; Kovacs, A. J.; Bassett, G. A.; Keller, A. *Kolloid-Z. Z. Polym.* **1966**, *209*, 115.
(3) Cogan, K. A.; Gast, A. P. *Macromolecules* **1990**, *23*, 745.
(4) Gast, A. P.; Vinson, P. K.; Cogan-Farinas, K. A. *Macromolecules* **1993**, *26*, 1774.
(5) Kawai, T.; Shiozaki, S.; Sonoda, S.; Nakagawa, H.; Matsumoto, T.; Maeda, H. *Makromol. Chem.* **1969**, *128*, 252.
(6) Droscher, M.; Smith, T. L. *Macromolecules* **1982**, *15*, 442.
(7) Gallot, B. Liquid Crystalline Order in Polymers. In *Liquid Crystalline Structure of Block Copolymers*; Blumstein, A., Ed.; Academic Press: New York, 1978; pp 192−235.
(8) Rangarajan, P.; Register, R. A.; Fetters, L. J. *Macromolecules* **1993**, *26*, 4640.
(9) Rangarajan, P.; Register, R. A.; Adamson, D. H.; Fetters, L. J.; Bras, W.; Naylot, S.; Ryan, A. *Macromolecules* **1995**, *28*, 1422.
(10) Douzinas, K. C.; Cohen, R. E.; Halasa, A. F. *Macromolecules* **1991**, *24*, 4457.
(11) Tirrell, M.; Patel, S.; Hadziioannou, G. *Proc. Natl. Acad. Sci. U.S.A.* **1987**, *84*, 4725.
(12) Factor, B. J.; Lee, L. T.; Kent, M. S.; Rondelez, F. *Phys. Rev. E* **1993**, *48*, R2354.
(13) Auvray, A.; Auroy, P. Scattering at Interfaces: Variations on Porod's Law. In *Neutron, X-Ray, and Light Scattering*; Lindner, P., Zemb, T., Eds.; Elsevier Science Publishers: Amsterdam, The Netherlands, 1991; pp 199−221.
(14) Vilgis, T.; Halperin, A. *Macromolecules* **1991**, *24*, 2090.
(15) Di Marzio, E. A.; Guttman, C. M.; Hoffman, J. D. *Macromolecules* **1980**, *13*, 1194.
(16) Birshtein, T. M.; Zhulina, E. B. *Polymer* **1990**, *31*, 1312.
(17) Whitmore, M. D.; Noolandi, J. *Macromolecules* **1990**, *23*, 3321.
(18) Khoury, F.; Passaglia, E. The Morphology of Crystalline Synthetic Polymers. In *Treatise on Solid State Chemistry*; Hannay, N. B., Ed.; Plenum Press: New York, 1976; Vol. 3, pp 335−496.
(19) Edwards, S. F. *Proc. Phys. Soc.* **1965**, *85*, 613.
(20) Hong, K. M.; Noolandi, J. *Macromolecules* **1981**, *14*, 727.
(21) Russel, W. B.; Saville, D. A.; Schowalter, W. R. *Colloidal Dispersions*; Cambridge University Press: Cambridge, Great Britain, 1989.
(22) Birshtein, T. M.; Zhulina, E. B. *Polymer* **1984**, *25*, 1453.
(23) Halperin, A.; Tirrell, M.; Lodge, T. P. *Adv. Polym. Sci.* **1992**, *100*, 31.
(24) Gervais, M.; Gallot, B. *Makromol. Chem.* **1973**, *171*, 157.
(25) Morton, M.; Fetters, L. J.; Inomata, J.; Rubin, D. C.; Young, R. N. *Rubber Chem. Technol.* **1975**, *49*, 303.
(26) Rosedale, J. H.; Bates, F. S. *J. Am. Chem. Soc.* **1988**, *110*, 3542.
(27) Bates, F. S.; Schulz, M. F.; Rosedale, J. H.; Almdal, K. *Macromolecules* **1992**, *25*, 5547.
(28) Russell, T. P. Small Angle Scattering. In *Handbook on Synchrotron Radiation*; Brown, G., Moncton, D. E., Eds.; Elsevier Science Publishers: Amsterdam, The Netherlands, 1991; Vol. 3, pp 379−469.
(29) Russell, T. P.; Lin, J. S.; Spooner, S.; Wignall, G. D. *J. Appl. Crystallogr.* **1988**, *21*, 629.
(30) Hammouda, B.; Krueger, S.; Glinka, C. J. *J. Res. Natl. Inst. Stand. Technol.* **1993**, *98*, 31.
(31) Howard, P. R.; Crist, B. *J. Polym. Sci., Part B: Polym. Phys.* **1989**, *27*, 2269.
(32) Tadokoro, H. *Structure of Crystalline Polymers*; John Wiley and Sons: New York, 1979.
(33) Hoffman, J. D.; Davis, G. T.; Lauritzen, J. I. The Rate of Crystallization of Linear Polymers with Chain Folding. In *Treatise on Solid State Chemistry*; Hannay, N. B., Ed.; Plenum Press: New York, 1976; Vol. 3, pp 497−614.
(34) Zirkel, A.; Richter, D.; Pyckhout-Hintzen, W.; Fetters, L. J. *Macromolecules* **1992**, *25*, 954.
(35) Vagberg, L. J. M.; Cogan, K. A.; Gast, A. P. *Macromolecules* **1991**, *24*, 1670.
(36) Berry, G. C. *J. Chem. Phys.* **1966**, *44*, 4550.
(37) Barton, A. F. M. *Handbook of Polymer−Liquid Interaction Parameters and Solubility Parameters*; CRC Press: Boca Raton, FL, 1990.
(38) Glatter, O.; Kratky, O. *Small Angle X-Ray Scattering*; Academic Press: New York, 1982.
(39) Wang, J. I.; Harrison, I. R. *J. Appl. Crystallogr.* **1978**, *11*, 525.
(40) Pilz, I. Proteins. In *Small Angle X-Ray Scattering*; Glatter, O., Kratky, O., Eds.; Academic Press: New York, 1982; pp 239−294.
(41) Chang, S. L.; Huang, J. S., private communication, 1995.
(42) Auroy, P.; Mir, Y.; Auvray, L. *Phys. Rev. Lett.* **1992**, *69*, 93.
(43) Auroy, P.; Auvray, L.; Leger, L. *Macromolecules* **1991**, *24*, 2523.

MA951871+